AGU PUBLICATIONS

JGR

Journal of Geophysical Research: Earth Surface

RESEARCH ARTICLE

10.1002/2013JF002826

Key Points:
- Channel incision relation to steepness calibrated from tilted bedrock surface
- Chlorine-36 exposure age dating shows bedrock surface exhumed at 1 to 2 m/kyr
- Low n values, consistent with shear stress ($n = 2/3$) satisfy field data

Supporting Information:
- Table S1
- Table S2
- Readme

Correspondence to:
M. E. Oskin,
meoskin@ucdavis.edu

Citation:
Oskin, M. E., D. W. Burbank, F. M. Phillips, S. M. Marrero, B. Bookhagen, and J. A. Selander (2014), Relationship of channel steepness to channel incision rate from a tilted and progressively exposed unconformity surface, *J. Geophys. Res. Earth Surface*, *119*, 366–384, doi:10.1002/2013JF002826.

Received 10 APR 2013
Accepted 9 JAN 2014
Accepted article online 13 JAN 2014
Published online 26 FEB 2014

Relationship of channel steepness to channel incision rate from a tilted and progressively exposed unconformity surface

M. E. Oskin[1], D. W. Burbank[2], F. M. Phillips[3], S. M. Marrero[3], B. Bookhagen[2], and J. A. Selander[1]

[1]Department of Earth and Planetary Sciences, University of California, Davis, California, USA, [2]Department of Earth Science, University of California, Santa Barbara, California, USA, [3]Department of Earth and Environmental Science, New Mexico Institute of Mining and Technology, Socorro, New Mexico, USA

Abstract We examine the relationship of channel steepness to incision rate from channels eroding into a previously tilted, planar, and progressively exhumed unconformity surface. Channel and unconformity slopes are measured from a suite of channels developed on erosionally resistant Paleozoic limestone exhumed by the removal of Cenozoic sediments from the Baybeiche Range bordering the Naryn basin in the western Tian Shan. The compiled data set, sampling 5 orders of magnitude of upstream drainage area (0.03 to 227 km^2), is used to derive the exponent, n, relating channel steepness to channel incision rate and the ratio, K/V, of the rate constant for channel incision of the resistant substrate, K, to the erosion rate, V, of the cover strata. We show that for a typical value of intrinsic concavity (slope-area exponent, $\theta = 0.5$), erosion rates that are proportional to specific stream power ($n = 1$) satisfy the data set. However, valley width data suggest that the intrinsic concavity is higher ($\theta = 0.8$) and that the channel incision data can also be fit if erosion is proportional to basal shear stress ($n = 2/3$). Our results do not support values of n significantly greater than one. Using ^{36}Cl exposure age dating of the unconformity surface, we independently demonstrate that the Cenozoic cover strata have been progressively stripped downward from the unconformity surface at a vertical rate of 1 to 2 m/kyr. Using $V = 1$ m/kyr, we constrain the rate constant, K, to between 6 ± 1 and $9 \pm 2 \times 10^{-4}$ kyr^{-1} for incision of resistant limestone bedrock in this field setting.

1. Introduction

Erosion by rivers is a primary mechanism by which landscapes adjust to climatic or tectonic forcing [*Beaumont et al.*, 1992; *Whipple and Tucker*, 1999] through the general dependence of bedrock channel incision on local riverbed steepness: the product of catchment area raised to a power, $\theta < 1$, with slope [*Howard*, 1994; *Whipple and Tucker*, 1999, 2002]. Incomplete knowledge of the functional form of fluvial bedrock erosion limits understanding of this response. Importantly, the degree of nonlinearity in the steepness dependence of fluvial bedrock erosion will determine the sensitivity of mountain range elevations to incision rate, and whether knickpoints or knickzones will retain their form [*Whipple and Tucker*, 2002], faithfully recording river response to changing boundary conditions [e.g., *Pritchard et al.*, 2009]. Potential feedbacks between sediment production, transport, flood frequency, channel width, and erosion via impact-abrasion may give rise to additional nonlinear effects on bedrock channel erosion [*Sklar and Dietrich*, 2004; *Lague et al.*, 2005; *Lamb et al.*, 2008; *Chatanantavet and Parker*, 2009].

Despite the many factors that affect fluvial bedrock incision [*Lague*, 2013], the distribution of river channel steepness in landscapes can be remarkably systematic [*Flint*, 1974; *Kirby and Whipple*, 2001; *Whipple*, 2004; *Ouimet et al.*, 2009; *DiBiase et al.*, 2010; *Wobus et al.*, 2006a; *Yanites and Tucker*, 2010]. Such patterns could arise because the essence of fluvial erosion is captured by a relatively simple function, such as stream power [*Howard*, 1994] or because thresholds in erosion rate or channel steepness must be crossed before more complex behavior, such as the formation of hanging valleys, is expressed in the landscape [*Crosby et al.*, 2007]. If a landscape is assumed to be in equilibrium with the rock uplift rate and base level, then channel steepness may be used to calibrate erosion rate laws [*Kirby and Whipple*, 2001; *Snyder et al.*, 2003; *Lague and Davy*, 2003; *Ouimet et al.*, 2009; *DiBiase et al.*, 2010]. Because the equilibrium assumption removes time-dependent effects from consideration, however, such landscapes may be ill-suited to identify which rate law is most appropriate. Time-dependent phenomena, such as the rate and form of knickpoint

propagation, may be better suited to discriminate among competing fluvial erosion models [*Whipple and Tucker*, 2002; *Whittaker et al.*, 2007; *Cowie et al.*, 2008]. Even in such cases, processes specific to knickpoints, such as plunge pool erosion [*Haviv et al.*, 2006] and the increased frequency of erosive discharge events [*Lague*, 2013], may dominate transmission of erosion signals upstream, compromising their utility.

Channel incision into a pristine, previously tilted, and progressively exposed bedrock surface offers an alternative, quasi steady state approach to testing and calibrating fluvial erosion rate laws. In such landscapes, the original slope of the surface imparts a strong imprint on river channel profile evolution [*Stock and Montgomery*, 1999; *Kooi and Beaumont*, 1996; *Goode and Burbank*, 2011]. Channel profiles cut into a progressively exposed surface are smoothly varying above the transition from cover strata to bedrock [*Oskin and Burbank*, 2007; *Goode and Burbank*, 2011], and thus less sensitive to erosion processes that are localized at the abrupt downstream transition from gentle to steep channel gradients at knickpoints. For the case of stream power, *Oskin and Burbank* [2007] found that both the form of channel profiles and the divergence of channel slopes relative to the initial condition are sensitive to the nonlinearity of the dependence of erosion with channel slope. Building on the analysis of *Oskin and Burbank* [2007], we present an expanded investigation of channel incision into resistant limestone bedrock progressively exposed from beneath a planar, tilted unconformity. We compare field and remote-sensing topographic surveys of channel and unconformity gradients to test the relationship of channel steepness to channel incision rate. Using cosmogenic ^{36}Cl, we directly date the exposure history of unconformity surface and thus simultaneously calibrate both the incision rate constant, K, and the steepness exponent, n, for this landscape.

2. Background

2.1. Channel Steepness and Erosion Rate

Channel steepness, k_s, describes the empirical relationship of channel slope, S_c, to catchment area, A,

$$S_c = k_s A^{-\theta}, \tag{1}$$

where the exponent θ is the intrinsic channel concavity [*Flint*, 1974]. Under conditions of uniform channel steepness, θ sets the upward concave shape of a graded stream channel profile [*Flint*, 1974; *Wobus et al.*, 2006a]. Typically in such settings it falls within a narrow range between 0.4 and 0.6 [*Tucker and Whipple*, 2002] though values as low as 0.3 [*Lague and Davy*, 2003] to as high as 1.0 [*Seidl and Dietrich*, 1992] have been documented. Both detachment-limited and transport-limited models of channel incision predict a monotonic and generally nonlinear relationship of channel slope to channel incision rate [*Whipple and Tucker*, 1999; , 2002; *Tucker and Whipple*, 2002],

$$E(S_c, A) = k_e[k_d k_s]^n, \tag{2}$$

where k_e is the erodibility or sediment transport coefficient of the channel, n is the steepness exponent, and k_d is a dimensional coefficient that casts the term in parentheses as specific stream power, or alternatively, in terms of shear stress if n is multiplied by 2/3. Combining (1) and (2) yields a prediction of channel steepness as a function of a uniform channel incision rate, E [*Whipple and Tucker*, 1999],

$$S_c = \left(\frac{E}{K}\right)^{\frac{1}{n}} A^{-\theta}, \tag{3}$$

where K is the product $k_e k_d^n$. Implicit in this approach is that a single effective discharge, proportional to A, controls the erosion rate. More realistically, a distribution of discharge events must be considered, along with a threshold for the onset of erosion [*Snyder et al.*, 2000; , 2003; *Tucker*, 2004; *Lague et al.*, 2005; *DiBiase and Whipple*, 2011]. Unfortunately information on the frequency of flood events is impossible to reconstruct for the geologic past. In terms of its effect, including realistic climatic variability tends to reduce the sensitivity of erosion rate to channel steepness because steeper rivers more frequently mobilize their bed load and exceed the threshold conditions for bedrock incision. Not including these effects results in a value for n that convolves the physics of the erosion process [*Hancock et al.*, 1998] with effects due to the frequency-magnitude distribution of geomorphically effective runoff events, resulting in significantly elevated effective n values [*Snyder et al.*, 2003; *Lague et al.*, 2005; *DiBiase and Whipple*, 2011].

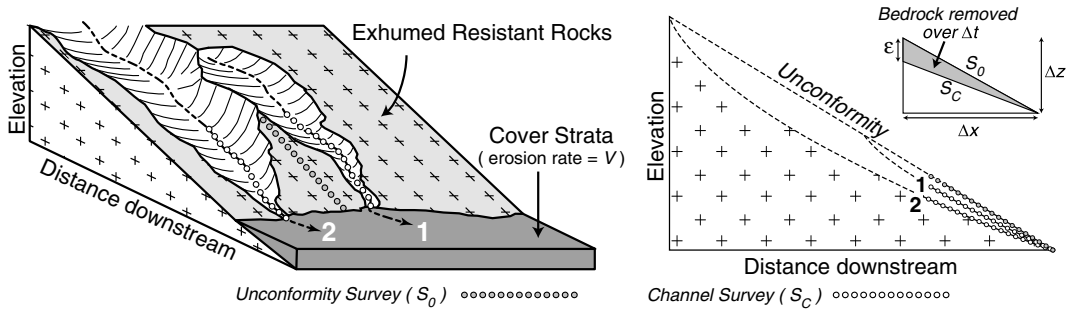

Figure 1. Schematic illustration of progressive exposure of resistant rocks via removal of cover strata at vertical erosion rate, V. Channel 1, with a larger upstream catchment area, will incise at a greater rate than channel 2. Cross-section view shows how channel profiles 1 and 2 compare. Surveys of the unconformity slope and the slope of the channels as they approach the contact with cover strata are used to determine relative rates of erosion as a function of catchment area and channel slope. ε is the amount of channel erosion over time Δt as a length Δx of the unconformity surface is exposed.

Deducing effective n values from natural landscapes requires examination of channel steepness across a range of erosion rates in order to empirically test the relationship in (2). *Snyder et al.* [2000] and *DiBiase et al.* [2010] took advantage of gradients in rock uplift rates in the Mendocino Triple Junction area and San Gabriel Mountains, respectively, in order to calibrate n. In these landscapes, it is reasonably assumed that erosion is in dynamic equilibrium with rock uplift, such that channel steepness can be extracted from analysis of the slope-area relationship in (1). *Kirby and Whipple* [2001] developed an approach that used gradients in erosion rate along individual channels crossing the Siwalik Hills to calibrate n. This possesses an advantage of minimizing the impact of climate gradients, which tend to covary with topography and complicate the interpretation of channel steepness across diverse landscapes. *Oskin and Burbank* [2007] showed how channel incision into a progressively exposed, resistant bedrock surface could also be used to calibrate n values within a compact field setting. In the next section, we review and generalize this method.

2.2. Incision of a Tilted Bedrock Surface

We extend the approach of *Oskin and Burbank* [2007] to any stream erosion rate rule, $E(X)$, where X is a set of parameters that may include channel slope, discharge, channel width, channel roughness, sediment flux, sediment caliber (size, hardness), or other variables. For simplicity, it is assumed that channels are cut directly down the bedrock slope, with negligible sinuosity, such that the problem is two-dimensional. It is further assumed that the bedrock contact is exposed at a steady rate. As resistant rocks are exposed (Figure 1), channels just upstream of the contact with cover strata are cut at a channel gradient, S_c that reflects the balance between the vertical rate of exposure of the contact from beneath the cover strata, V, the contact slope, S_0, and the local vertical channel incision rate into the underlying resistant rocks, $E(X)$. From this geometry, we derive a quasi steady state solution for ratio of the channel incision rate to the vertical rate of exposure of the contact.

Consider a finite increment of channel incision, ε, over an increment of time Δt during which a thickness of cover strata, Δz, is removed,

$$\Delta z = V \Delta t. \tag{4}$$

Over the same time interval, the amount of bedrock channel incision,

$$\varepsilon = E(X)\Delta t. \tag{5}$$

Eliminating Δt yields

$$\varepsilon = \frac{E(X)}{V}\Delta z. \tag{6}$$

As shown graphically in Figure 1, channel incision lowers the channel slope from S_0 to S_c,

$$S_c = \frac{\Delta z - \varepsilon}{\Delta x}. \tag{7}$$

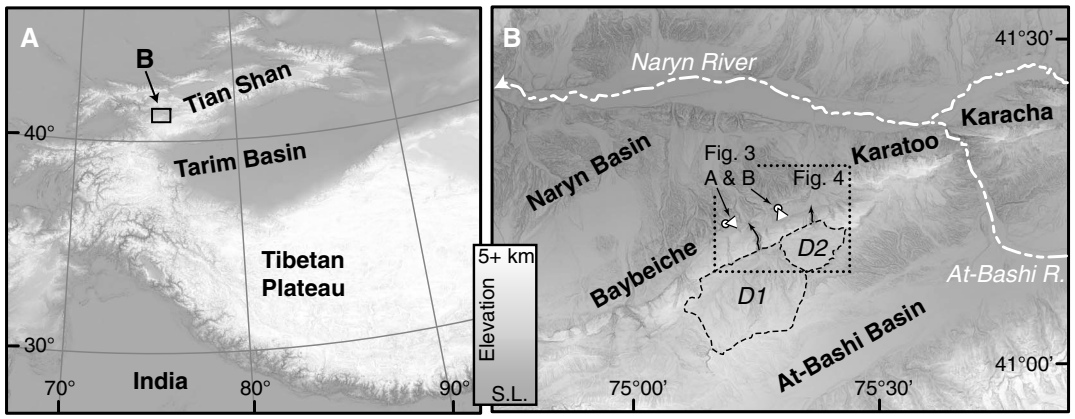

Figure 2. (a) Index map of Central Asia, showing the location of the Naryn-At Bashi basin within the western Tian Shan. (b) Digital elevation model of the Naryn-At Bashi basin showing the location of the Baybeiche-Karatoo-Karacha folds. Locations shown for field photos (Figure 3) and map (Figure 4). The largest catchment surveyed, D1, has a source area that extends beyond Figure 4, as shown.

By substitution of (6) into (7), and S_0 for $\Delta z/\Delta x$,

$$S_c = S_0\left(1 - \frac{E(X)}{V}\right). \tag{8}$$

Rearranging (8), we define a dimensionless channel incision rate, I, by normalizing the bedrock incision rate by the vertical rate of removal of the cover strata,

$$I = \frac{E(X)}{V} = 1 - \frac{S_c}{S_0}. \tag{9}$$

By measuring channel gradients S_c, formed by catchments of various areas incised below contacts of different initial dips, S_0, or exposure rates, V, it is possible to design natural experiments to test the validity and explore the functional form of particular stream channel erosion rate laws. The advantage of this approach is that it is straightforward to compare many adjacent channels developed under common boundary conditions of climate, lithology, and exhumation rate, while varying catchment area and contact slope (Figure 1). For small catchment areas where channel slope, S_c, does not diverge substantially from the unconformity slope, S_0, the dimensionless incision rate, I, is highly sensitive to the slope measurements. Thus, detailed field topographic surveys prove necessary to apply this model over a sufficient range of catchment areas to sample an adequate span of channel steepness values [*Oskin and Burbank*, 2007]. Ideally the catchment area should not increase substantially over the reach where slopes are measured, nor over the time interval represented by its exposure. Both conditions are well met for short channel reaches, so long as no large tributaries are introduced, and the upstream drainage network evolves slowly relative to the rate of exposure of the contact.

2.3. Exhumed Unconformity in the Tian Shan

We develop a natural experiment to examine the relationship of channel steepness to incision rate using a progressively exposed unconformity surface in the Tian Shan of Central Asia. The Tian Shan (Figure 2) is an active orogen that absorbs up to 20 mm/yr of convergence [*Abdrakhmatov et al.*, 1996]. Prior to the onset of shortening, a beveled bedrock plain of very low relief existed over the region [*Davis*, 1904; *Chediya*, 1986; *Burbank et al.*, 1999]. Where buried by younger foreland basin deposits, this plain now forms a planar unconformity separating Cenozoic nonmarine strata from Paleozoic and older bedrock. Because the Cenozoic cover strata erode much more readily than the underlying Paleozoic rocks, erosion tends to exhume the unconformity to form prominent, low-relief topographic surfaces visible across the landscape.

Remnants of exhumed unconformity are widely exposed on the north facing slopes of four south vergent folds in the central Naryn-At Bashi basin (Figure 3). These en echelon structures underlie a topographic ridge line separating the Naryn subbasin, to the north, from the At-Bashi subbasin, to the south. In the prevailing semiarid climate, Paleozoic carbonate rocks exposed in the cores of these folds are exceptionally erosion resistant, forming broad, north tilted panels on the fold back limbs reaching elevations in excess of 3.5 km [*Burbank et al.*, 1999]. Cenozoic cover strata are concordant to the underlying unconformity surface and

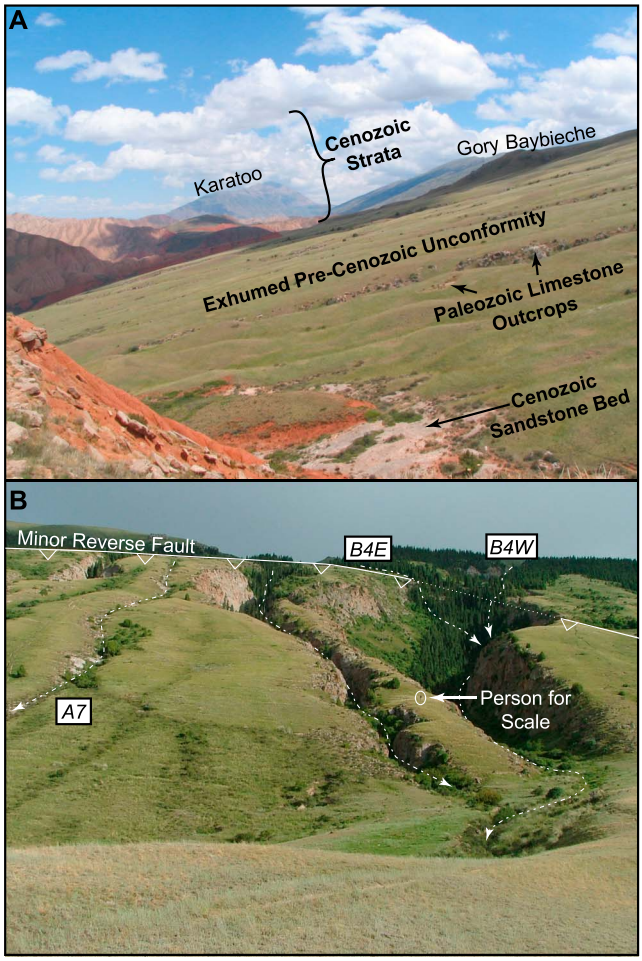

Figure 3. (a) View east along contact between Cenozoic strata and Paleozoic limestone. The exhumed pre-Cenozoic unconformity and overlying Cenozoic rocks dip 21° in the proximal portion of the photograph. Crests of Gory Baybeiche and Karatoo folds visible in the background. (b) Photo of the base of the exhumed unconformity surface showing examples of streams surveyed for this study. A minor reverse fault that offsets the exhumed unconformity surface cuts obliquely across the field of view. Minor faults such as this impact the formation of channels as the unconformity is exhumed: Channel A7 begins just downslope of this fault; runoff from channels B4W (west tributary) and B4E (east tributary) appear to join at the fault trace, reflecting stream piracy that was possibly triggered via subsurface flow along the fault trace.

show that no significant tilting of these fold limbs occurred during filling of the Naryn-At Bashi basin with fluvial and lacustrine sediments. Folding with reverse faulting appears to have begun in the Pliocene or Quaternary, and deformed terraces indicate ongoing late Quaternary uplift [*Goode*, 2011]. This uplift appears to be primarily accommodated by translation of the folds above an en echelon, north dipping reverse fault system that crops out to the south of the fold belt, with material deformed through a synclinal fault bend fold axis located approximately 3 to 5 km north of the limestone-cover strata contact. Based on the limited extent of tilted late Quaternary terraces near this fold axis, the structural interpretation of *Goode and Burbank* [2011] shows little to no active steepening of the folds in the vicinity of the limestone outcrops. Small faults and subtle warping deform the unconformity surface and, where observable, cut the cover strata as well.

Three Cenozoic formations are progressively exposed and eroded prior to exhumation of the unconformity and underlying Paleozoic rocks. The Kokturpak formation immediately overlies the unconformity. It comprises a thin veneer (generally <5 m) consisting of red, gypsiferous mudstone alternating with red-to-pink colored, poorly sorted sandstone and conglomerate. Uncommon, highly weathered basalt flows also occur within the Kokturpak formation [*Sobel and Arnaud*, 2000]. In many areas, the Kokturpak formation consists solely of a relict soil horizon developed onto weathered regolith of underlying carbonate rocks. The Shamsi formation immediately overlies the Kokturpak formation and consists of alternating mudstone and fine-to-coarse sandstone with uncommon conglomerate lenses. Sandy units give way to a greater proportion of silty mudstone up section. The Shamsi formation is characterized by a red color that gradually fades to light reddish tan up section. The thickness of the Shamsi formation is approximately 500 m in the study area [*Goode et al.*, 2011]. The Shamsi formation is overlain by tan mudstone and siltstone of the Chu formation. The thickness of the Chu formation is not well determined but must be at least 2 km in the vicinity of the study area [*Goode and Burbank*, 2011].

Age control is generally poor for the Neogene units of the Tian Shan. The Shamsi and Chu formations have been identified in several Neogene basins, primarily on the basis of the red color of the Shamsi formation. The Shamsi-Chu contact has been dated to 7 Ma in the Kochkor basin with magnetostratigraphy and fossil control [*Abdrakhmatov et al.*, 2001]. However, because the color transition between Shamsi and Chu for-

mations may not represent a time horizon, and because the basins of the northern Tian Shan were likely isolated from the Naryn-At-Bashi basin, it is unclear whether this age may be applied to the Shamsi-Chu contact in the study area. Cooling ages from the At-Bashi range that bounds the southern margin of the basin suggest the onset of uplift and erosion some time after approximately 25 Ma [*Sobel and Dumitru*, 1997], which is significantly older than for the northern Tian Shan [*Bullen et al.*, 2001; *Sobel et al.*, 2006]. Thus, though the age of burial of the unconformity is not well constrained, it has likely been covered since at least the middle to late Miocene.

Currently, almost the entire Naryn-At Bashi basin is undergoing erosion by the Naryn river system (Figure 2). Extensive badland topography with modest (100 to 500 m) local topographic relief characterizes exposures of Cenozoic strata. Higher topography and relief occur where cover strata have been removed and Paleozoic rocks crop out along the en echelon folds across the central part of the basin. The contact of Cenozoic rocks on Paleozoic rocks is marked by a triangular outcrop pattern (cuestas) of Cenozoic strata. This rugged topography along the contact suggests that erosion is continuously exposing the Paleozoic rocks in the core of these folds. Contrasting channel patterns indicate that the arrangement of the channel network is strongly affected by removal of the cover strata to expose the limestone bedrock. Channels within the cover strata form a trellis network. Steep, dendritic low-order streams feed into a quasi-parallel array of higher-order axial channels characterized by flights of cut-fill terraces. A transition in the drainage network appears where the erosion exposes the tilted unconformity surface. Where the axial channels cross the unconformity, these axial channels correspond to deeply incised gorges with large upstream catchment areas in the Paleozoic rocks. This pattern suggests that these larger drainages are simply inset into the more resistant Paleozoic rocks as these rocks are progressively exposed by erosion of the Cenozoic cover strata. This pattern contrasts with that of the lower-order tributary drainages. As Paleozoic rocks are exposed by the lowering of the boundary between the Cenozoic and Paleozoic rocks, these smaller drainages appear to be reorganized into a set of parallel, modestly incised channels oriented down the slope of the unconformity surface.

3. Methods

3.1. Channel Surveys

Streams incised into the Baybeiche range were selected for detailed study (Figure 4) because this fold displays the longest strike length and least-tilted fold back limb among the four en echelon folds that divide the Naryn basin from the At-Bashi basin (Figure 2). Elevation surveys for most streams were collected in the field using differential GPS (Figure 5) or a portable laser range finder (Figure 6) just above where these channels drain from the Paleozoic rocks across the unconformity into Cenozoic strata (Figure 4). The unconformity surface was also surveyed along immediately adjacent channel interfluves. Channel survey resolution and error vary with the types of instruments employed. Differential GPS surveys were conducted with a pair of Trimble GeoXT handheld instruments, with one set up as a local base station. These data were post-processed to a yield differentially corrected elevations. Vertical precision of most points was 0.5 m, although point-to-point precision demonstrated by the continuity of surveyed profiles (Figure 5) is significantly better than 0.5 m. Laser rangefinder surveys were acquired with a Lasercraft Contour XLRic handheld reflectorless instrument. Distance and angle measurements reported by this instrument are to within 0.1 m and 0.1°, respectively, with good repeatability of measurements. Additional channel and unconformity profiles were extracted from satellite-derived topography (Figure 7), either produced from a stereo pair of 2.5 m pixel SPOT5 imagery, or from 3 arc second Shuttle Radar Topography Mission data [*Farr et al.*, 2007]. All catchment areas were digitized from SPOT5 imagery. Larger catchment areas were checked with flow routing over available digital topographic data.

Channel width data were not systematically collected in the field. In order to evaluate the role of channel width in controlling the pattern of incision, incised valley floors were digitized as polygons using 2.5 m resolution SPOT5 data (see file valleyfloorpolygons.zip in the supporting information). Incised valley walls were identified from rock outcrops, cliffs, and sparser vegetation. The width of each digitized polygon encompasses the entire portion of the valley that has been directly subject to lowering by fluvial erosion. Valley floor width is usually greater than the width of the active channel that may be defined from field evidence for recent scour and fluvial sediment transport. Valley widths were computed every meter from the polygon width according to the algorithm of *Fisher et al.* [2013]. These data were compiled as moving averages over 10 m intervals, and are reported as a mean value and one standard deviation of these averaged values.

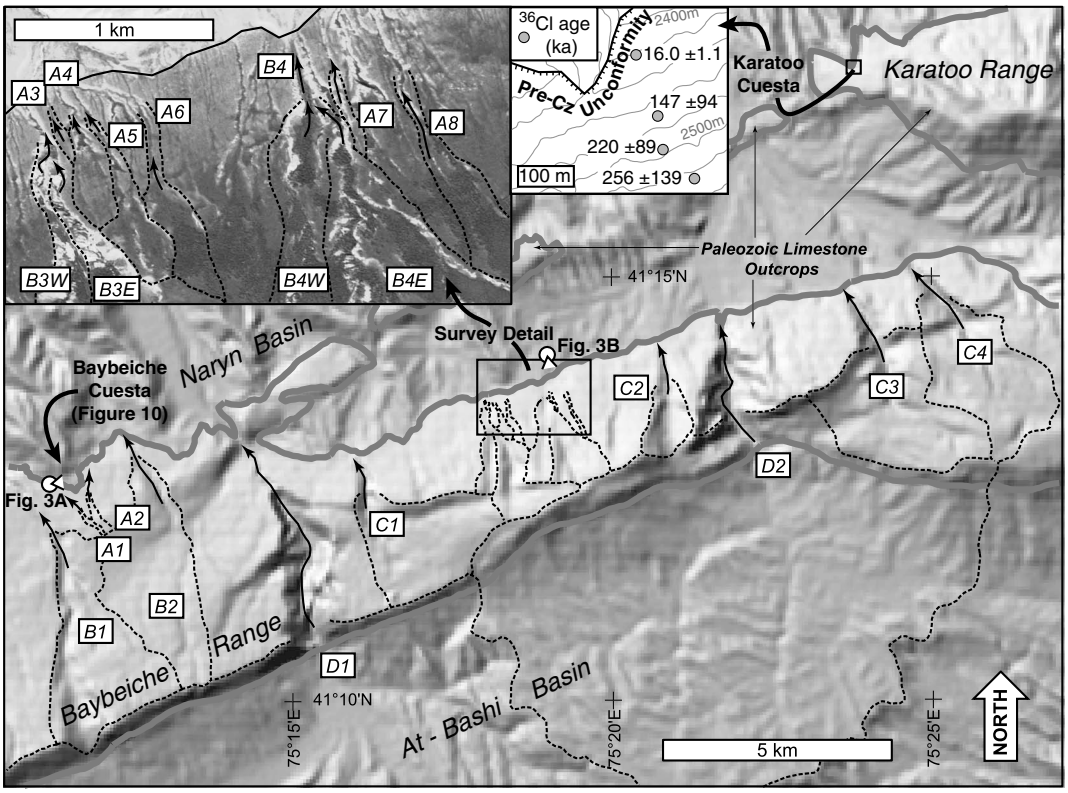

Figure 4. Map of location of channel surveys on north dipping limb of Gory Baybeiche. Dotted lines show digitized extent of upstream catchment areas. Channels surveys A1–A8 from differential GPS (Figure 5), B1–B4 from a laser rangefinder (Figure 6), C1–C4 and D1–D2 from satellite-derived topography (Figure 7). Inset at top left shows survey details on SPOT-5 image base. Inset top center shows ^{36}Cl exposure ages of exhumed planar unconformity surface at Karatoo Cuesta site. ^{36}Cl exposure ages for the Baybeiche Cuesta site shown in Figure 10.

Slopes for stream channels and adjacent sections of the unconformity surface were computed from survey data immediately above the contact with cover strata. Portions of streams crossing small faults and changes in dip of the unconformity surface were avoided in selecting reaches for slope measurement. All of the survey results are projected onto profiles oriented along the dip direction of the unconformity. Slopes with 95% confidence intervals were derived via linear regression of points on the channel thalweg and on the adjacent unconformity surface at the interfluves. Due to the low resolution of the Shuttle Radar Topography Mission data, some elevation points are above the canyon floor. Where possible, these points were excluded (Figure 7).

3.2. ^{36}Cl Exposure Age Dating

In order to independently verify progressive exposure of the unconformity surface and to calibrate the erodibility of the Paleozoic rocks, cosmogenic ^{36}Cl exposure age samples were collected near the contact between limestone bedrock and the cover strata. The results from this suite of ages should reflect lowering of the badland topography formed by erosion into the Cenozoic rocks, thereby exposing the Paleozoic limestone progressively from south to north. ^{36}Cl samples were processed at New Mexico Tech using a modified version of the procedure in *Marrero* [2012]. Samples were cleaned of any organic material, crushed and sieved to obtain the 250–1000 microns fraction, and leached in dilute (3–5%) nitric acid for 8–10 h. Aliquots for analysis of major oxides by X-ray fluorescence (XRF) and trace elements by inductively coupled plasma optical emission spectroscopy (ICP-OES) (shown in Table S1 in the supporting information) were taken off using a sample splitter. Samples were dissolved using concentrated hydrofluoric and nitric acids, in the case of silicate rocks, or only nitric acid, in the case of limestone or dolomite. A spike of nearly pure ^{35}Cl was added at the beginning of the dissolution. After separation of the dissolution residue by centrifugation, the accelerator mass spectrometer (AMS) target material, AgCl, was precipitated overnight on a warm plate and then collected by centrifuging. ^{36}S constitutes an interfering isobar during the AMS analysis of ^{36}Cl, and

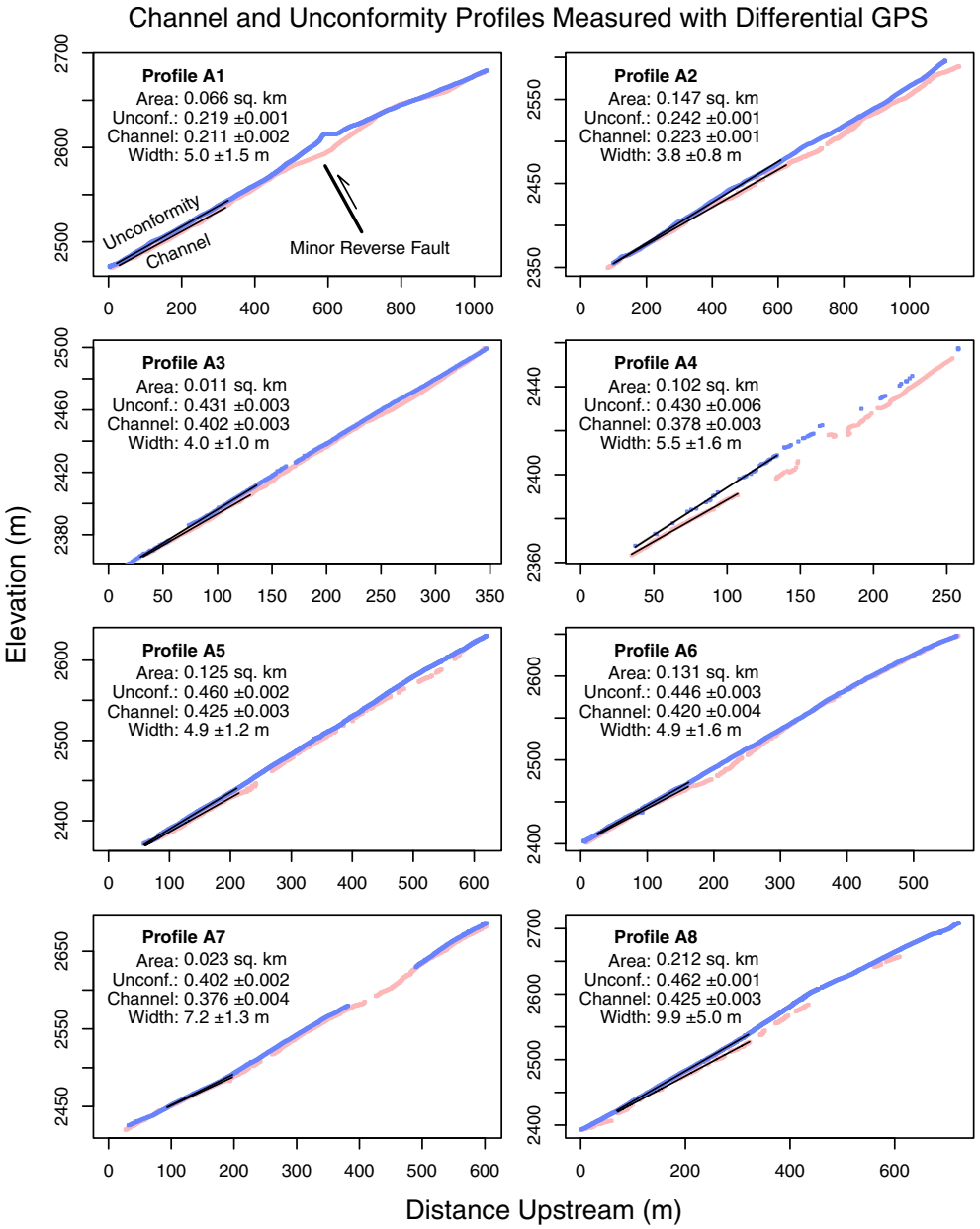

Figure 5. Channel and unconformity surveys for channels A1–A8. Upstream catchment area, best-fitting slopes (± 95% confidence) for channel outlet and unconformity and valley width ($\pm 1\sigma$) shown for channel. Unconformity points blue and channel points red. Note the locally deeper channel incision in profile A1 across a minor reverse fault that offsets the unconformity surface.

therefore it was removed by means of barium nitrate precipitation. The precipitate was separated using a syringe filter. After purification and drying, the samples were packaged and shipped to the PRIME Lab (Purdue University) for AMS analysis. Chlorine concentration was determined during the AMS analysis by means of isotope dilution mass spectrometry on the combined isotopically labeled spike Cl and sample Cl [*Desilets et al.*, 2006]. Calculated values of ^{36}Cl concentration (at/g) and Cl concentration (ppm) are given in Table S1.

Exposure ages (Table 1) were calculated with 5, 7.5, 10, and 25 mm/kyr surface lowering rates using the CRONUS calculator for ^{36}Cl (http://www.cronuscalculators.nmt.edu). The ages were calculated using the scaling method of *Lifton et al.* [2013]. The sea level, high-latitude production rates were as follows: spallation of K, 157 ± 6 atoms ^{36}Cl (g K)$^{-1}$ yr^{-1}; spallation of Ca, 56.0 ± 2.2 atoms ^{36}Cl (g Ca)$^{-1}$ yr^{-1}; low-energy neutrons, 704 ± 141 neutrons (g air)$^{-1}$ yr^{-1} [*Marrero*, 2012]. Age uncertainties are relatively large because for

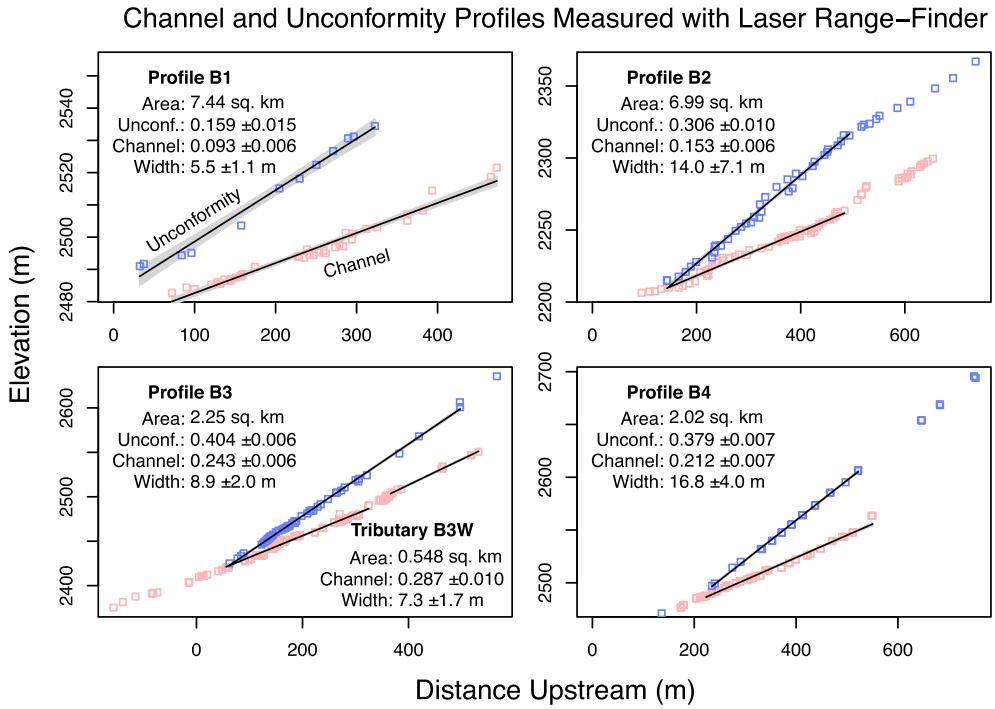

Figure 6. Channel and unconformity surveys for channels B1–B4. Upstream catchment area, best-fitting slopes (± 95% confidence) for channel outlet and unconformity and valley width ($\pm 1\sigma$) shown for each channel. Unconformity points are in blue and channel points in red.

most of the samples, the production by low-energy neutron absorption reactions was 25 to 75% of the total production, and the uncertainty associated with this production pathway is large.

4. Results

4.1. Channel Measurements

Elevation surveys of 12 channels and the adjacent unconformity surface, with upstream catchment areas ranging from 0.03 to 7.4 km^2, were collected in the field (Figure 5 and 6). To this data set, we add slope and area data from satellite-derived topography (Figure 7) for six additional drainages with catchment areas ranging from 1.4 to 227 km^2. Thus, the data set overall, summarized in Table 2, includes catchment sizes ranging over 5 orders of magnitude. Local slopes of the unconformity surface range from 0.16 to 0.46 (9 to 25°) with incised channel thalweg slopes of 0.063 to 0.43 (4 to 23°). The differential slope between the unconformity and channels—a raw measure of the efficiency of channel incision relative to the exhumation rate of the unconformity—ranges from 0.0082 to 0.25 (0.5 to 14°) and generally increases with upstream catchment area, showing that channels with larger discharge incise more rapidly (Figure 8). Note that the points with area, $A > 0.5$ km on Figure 8 appear to group into two trends. The upper trend, indicating more erosion for streams as a given catchment area, is dominated by channels incised into more steeply sloped portions of the unconformity, with $S_0 \geq 0.35$ (19°). This supports the contention that channels with greater slope erode more effectively.

Channel morphology and valley width qualitatively vary with catchment size. The smallest surveyed channels (catchment area $<$ 0.5 km^2) form shallow, vegetation-filled troughs less than 5 m across (e.g., channel A7 on Figure 3). Small fans with coarse, angular clasts are recognizable at the outlets of some of these channels, suggesting sediment transport by debris flows. Intermediate-sized channels occupy narrow incised valleys, 5 to 25 m wide, framed by steep to vertical walls cut into the limestone bedrock (e.g., channel B4 on Figure 3B). Axial channels within these valleys are 2 to 4 m across, less vegetated than surrounding valley floors, and consist primarily of exposed bedrock steps controlled by bedding in the limestone, with occasional pockets of loose gravel. The largest channels (catchment area $>$ 10 km^2) occupy wide ($>$ 30 m) valleys mantled by subrounded limestone cobbles and boulders. The active channel often occupies the entire width of the incised valley floor.

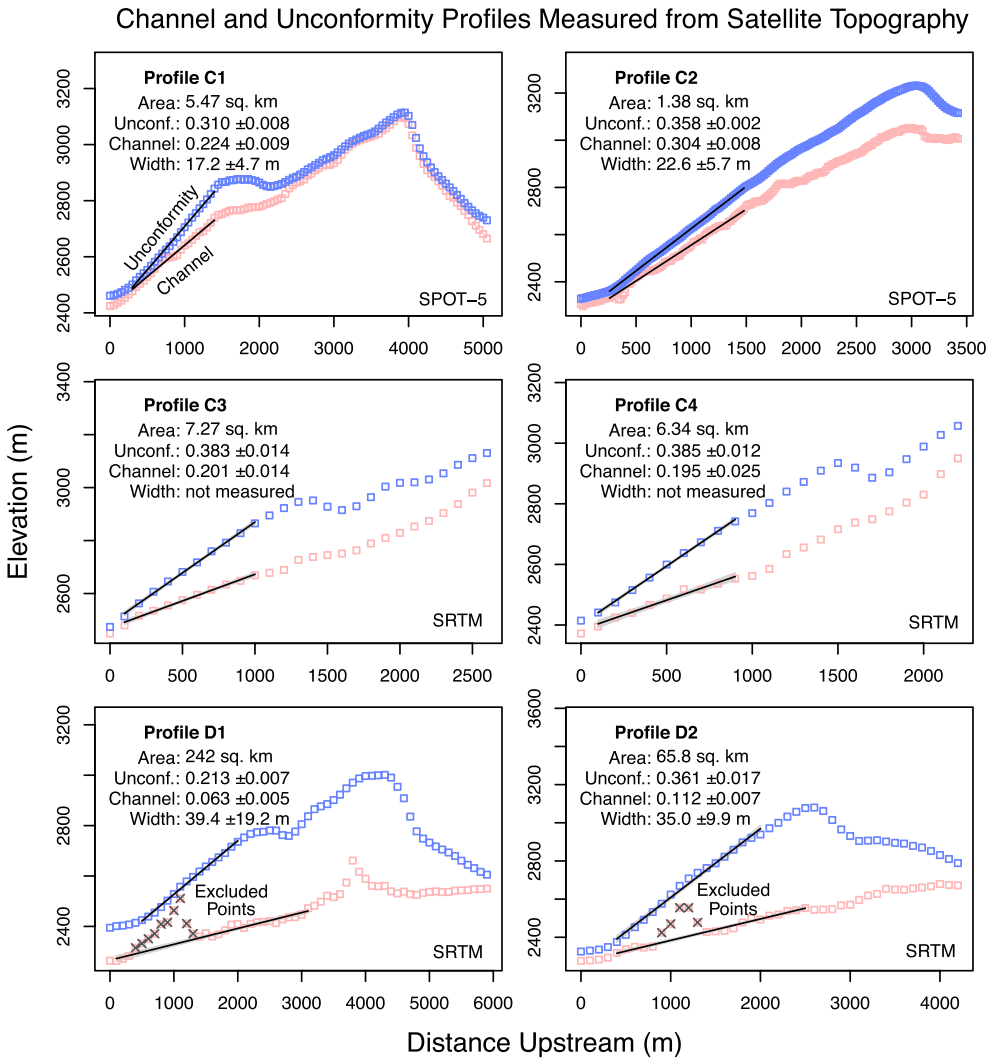

Figure 7. Channel and unconformity topographic profiles for channels C1–C4 and D1 and D2. Channels C1 and C2 data derived from stereo SPOT-5 imagery. Other channels from Shuttle Radar topography. Upstream catchment area, best-fitting slopes (± 95% confidence) for channel outlet and unconformity, and valley width ($\pm 1\sigma$) shown for each channel. Unconformity points are in blue and channel points in red.

Quantitative measurements of incised valley floor width yield a positive relationship with catchment area (Figure 9), similar to the relationship of channel width to catchment area found for bedrock rivers [*Whipple*, 2004]. The scaling exponent we find for valley width, 0.2 ± 0.1 (Figure 9), is slightly below the empirically determined range of 0.3 to 0.5 suggested by *Whipple* [2004] for bedrock channel width, but within the range of values found in other studies [*DiBiase and Whipple*, 2011; *Lague*, 2013].

4.2. Exposure Ages

Twelve limestone samples were collected from the unconformity surface surrounding a 21° north northeast dipping cuesta of Cenozoic strata on the north limb of the Baybeiche range (white points on Figure 10). To this data set, we add four samples collected from a similar setting on the adjacent Karatoo range where the cover strata dip 24° (Figure 4, inset). With two exceptions, limestone ^{36}Cl exposure ages increase away from the unconformable contact between Paleozoic and Cenozoic strata. One age (46 ± 7 kyr on Figure 10) appears too young due to erosion of the limestone outcrop. This sample site sits immediately adjacent to a channel incised into the limestone, and could be impacted by physical erosion. One anomalously old age (69 ± 15 kyr on Figure 10) is situated very close to unconformity contact. The origin of this age is puzzling, but could have been caused by local scouring of a channel down to the Paleozoic rocks 100–200 m ahead of the advancing main wave of stripping of the Cenozoic strata.

Table 1. Chlorine-36 Sample Location and Analysis Summary[a]

Name	Latitude	Longitude	Elev.	Shield.	Thick.	[36Cl]	Error	Exposure Ages (kyr) for Various Surface-Lowering Rates			
-	(dd)	(dd)	(m)	-	(cm)	(atoms/g)	(atoms/g)	5 mm/kyr	7.5 mm/kyr	10 mm/kyr	25 mm/kyr
KYR04-01	41.20947	75.19409	2449	0.984	3.0	62068	10402	2.2 ± 0.9	2.1 ± 0.8	2.1 ± 0.8	1.9 ± 0.6
KYR04-02	41.20947	75.19421	2451	0.940	4.0	70108	7269	2.3 ± 0.6	2.3 ± 0.7	2.2 ± 0.7	2.0 ± 0.6
KYR04-03	41.20942	75.19427	2452	0.942	4.0	127809	19280	3.9 ± 1.2	3.8 ± 1.1	3.7 ± 1.0	3.3 ± 0.7
KYR04-04	41.20938	75.19440	2455	0.984	4.5	446789	21766	13.6 ±2.7	12.8 ± 2.5	12.3 ± 2.3	10.8 ± 2.5
KYR04-05	41.20910	75.19470	2569	0.996	3.0	1198228	37667	31.2 ± 5.8	29.7 ± 5.7	29.0 ± 5.8	33.2 ± 11.8
KYR04-06	41.20883	75.19540	2484	0.990	2.5	14403750	328565	64.1 ± 9.6	68.8 ± 15.3	79.4 ± 25.5	EC
KYR04-07	41.20885	75.19630	2495	0.995	2.5	5900796	146379	29.0 ± 3.1	28.6 ± 3.5	28.6 ± 3.8	36.9 ± 10.3
KYR04-08	41.20868	75.19700	2508	0.995	3.0	14230056	514576	48.8 ± 9.6	48.2 ± 11.0	49.6 ± 13.6	EC
KYR04-09	41.20779	75.19791	2531	1.990	2.0	9153037	287629	44.9 ± 4.8	46.3 ± 6.6	49.3 ± 8.9	EC
KYR04-10	41.21186	75.19627	2425	0.993	5.0	2126076	117398	16.7 ±1.1	17.0 ±1.2	17.4 ± 1.4	20.9 ± 2.1
KYR04-11	41.21125	75.19781	2452	0.994	1.5	5168221	145490	35.3 ±2.4	36.6 ± 3.0	38.5 ± 3.8	EC
KYR04-12	41.21090	75.19915	2467	0.995	3.0	9877006	284439	79.5 ±11.3	97.7 ± 19.7	146.4 ± 83.8	EC
KYR04-13	41.20946	75.19815	2496	0.998	4.0	17051836	409563	53.3 ± 10.9	53.2 ± 13.1	55.6 ± 16.1	EC
KYR04-14	41.20821	75.19637	2511	0.998	5.0	20249977	897340	45.9 ± 9.1	45.0 ± 10.1	45.7 ± 12.2	EC
KYR04-15	41.20783	75.19552	2513	0.997	2.0	17318522	480419	62.7 ± 11.0	64.6 ± 14.3	70.7 ± 21.7	EC
KYR04-16	41.20754	75.19471	2515	0.996	4.0	5991520	251865	33.1 ± 3.1	33.6 ± 3.5	34.7 ± 4.2	69.5 ± 46.9
KYR04-18	41.20772	75.19432	2508	0.995	4.5	5217961	254133	17.0 ± 2.6	16.3 ± 2.6	15.8 ± 2.6	15.2 ± 3.2
KYR04-22	41.29505	75.41085	2477	0.981	1.0	31701209	1050121	114.4 ± 32.8	147.3 ± 94.4	EC	EC
KYR04-23[b]	41.29451	75.41097	2510	0.981	3.0	26305738	719240	EC	EC	EC	EC
KYR04-24[b]	41.29403	75.41165	2539	0.980	4.0	25136325	745863	EC	EC	EC	EC
KYR04-30	41.29603	75.41035	2422	0.950	1.5	1847113	89628	15.7 ± 1.0	16.0 ± 1.1	16.4 ± 1.2	19.7 ± 2.0

[a]EC = excess concentration (i.e., measured ^{36}Cl in excess of secular equilibrium at the assumed erosion rate).
[b]KYR04-23 is 220 ± 89 ka and KYR04-24 is 256 ± 139 ka with 3 mm/kyr surface-lowering rate.

Coarse sandstone beds that punctuate the lower Shamsi formation (Figure 3) create resistant, dipping shelves in the landscape. In order to further test the hypothesis that the Baybeiche cuesta has formed by progressive northward stripping of the cover strata, we collected exposure age samples from a one of these sandstone beds (black points on Figure 10). Presuming that the lowering rate of the fine-grained Cenozoic strata is more or less the same above and below this bed, then the resistant bed should emerge from its upper contact at a rate that is similar to rate of exposure of the underlying contact between the limestone and the cover strata. Five closely spaced samples were collected. Distances from each sample to the adjacent sandstone/mudstone contact were measured with a tape in the field. Like the limestone samples, the sandstone also displays progressively increasing ages away from the contact with overlying strata.

Table 2. Summary of Channel Survey Data

Name	Latitude (dd)	Longitude (dd)	Catchment (sq. km)	Channel Slope	Unconformity Slope	Valley Width (m)
A1	41.20564	75.19340	0.066	0.211 ± 0.002	0.219 ± 0.001	5.0 ± 1.5
A2	41.21011	75.19678	0.147	0.223 ± 0.001	0.242 ± 0.001	3.8 ± 0.8
A3	41.22549	75.30224	0.011	0.402 ± 0.003	0.431 ± 0.003	4.0 ± 1.0
A4	41.22554	75.30389	0.102	0.378 ± 0.003	0.430 ± 0.006	5.5 ± 1.6
A5	41.22540	75.30572	0.125	0.425 ± 0.003	0.460 ± 0.002	4.9 ± 1.2
A6	41.22679	75.31146	0.131	0.420 ± 0.004	0.446 ± 0.003	4.9 ± 1.6
A7	41.22816	75.31817	0.023	0.376 ± 0.004	0.402 ± 0.002	7.2 ± 1.3
A8	41.22871	75.32008	0.212	0.425 ± 0.003	0.462 ± 0.001	9.9 ± 5.0
B1	41.20186	75.18567	7.44	0.093 ± 0.006	0.159 ± 0.015	5.5 ± 1.1
B2	41.21406	75.20339	6.99	0.153 ± 0.006	0.306 ± 0.01	14.0 ± 7.1
B3	41.22556	75.29877	2.25	0.243 ± 0.006	0.404 ± 0.006	8.9 ± 2.0
B3W	41.22319	75.29948	0.548	0.287 ± 0.01	0.404 ± 0.006	7.3 ± 1.7
B4	41.22868	75.31441	2.02	0.212 ± 0.007	0.379 ± 0.007	16.8 ± 4.0
C1	41.21561	75.26648	5.47	0.224 ± 0.009	0.310 ± 0.008	17.2 ± 4.7
C2	41.23689	75.34569	1.38	0.304 ± 0.008	0.358 ± 0.002	22.6 ± 5.7
C3	41.24654	75.39467	7.27	0.201 ± 0.014	0.383 ± 0.014	-
C4	41.25104	75.41158	6.34	0.195 ± 0.025	0.385 ± 0.012	-
D1	41.21503	75.24056	242	0.063 ± 0.005	0.213 ± 0.007	39.4 ± 19.2
D2	41.24236	75.36183	65.8	0.112 ± 0.007	0.361 ± 0.017	35.0 ± 9.9

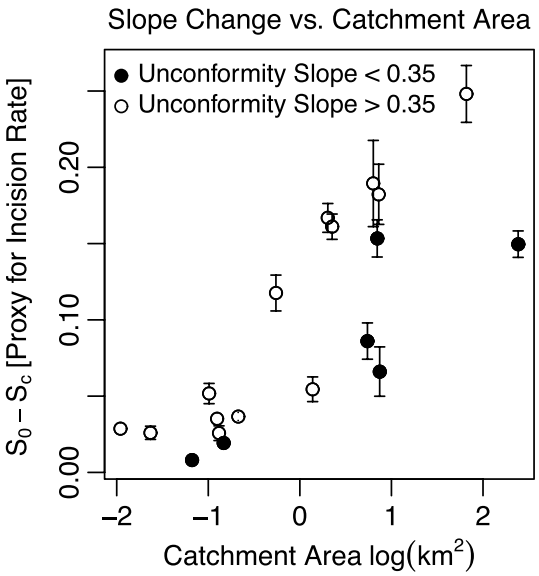

Figure 8. Semilog plot of the difference between unconformity slope and channel slope—a proxy for canyon incision rate—versus catchment area. Black points denote channels formed on portions of the exhumed unconformity that dip <0.35 (19°).

5. Discussion

5.1. Analysis of Channel Steepness

Correlation of channel incision rate with channel steepness empirically constrains the form of the channel incision rate law in (2). Combining equations (2), (3), and (9),

$$I = \frac{K}{V} k_s^n. \tag{10}$$

Recall that K is the product, $k_e k_d^n$, and $k_s = A^\theta S_c$ from rearrangement of (1). Taking the logarithm of both sides,

$$\log(I) = \log\left(\frac{K}{V}\right) + n\log(k_s), \tag{11}$$

defines a linear log-log relationship with slope, n, and an intercept value at $\log(k_s) = 0$ where the ratio of terms, K/V, is unity. Figure 11 shows the correlation of all channel results for a typical value of intrinsic channel concavity, θ, of 0.5. As expected, there is a positive correlation of incision rate to steepness ($R^2 = 0.65$). The slope of the relationship defines an n value close to unity (0.9 ± 0.3 at 95% confidence). The intercept value defines K/V that is also close to unity within 95% confidence. This intercept happens to occur close to the two data points with the largest channel steepness. These correspond to the two largest rivers included in our study, with dimensionless incision rates of ~0.7.

In order to incorporate channel or valley width into the analysis, we apply the well-known stream power model [*Howard*, 1994]. Specific stream power describes the power expenditure per unit area of the river bed as a function of channel slope, S_c, characteristic discharge, Q_w in m^3/yr, and channel or valley width, W, in m,

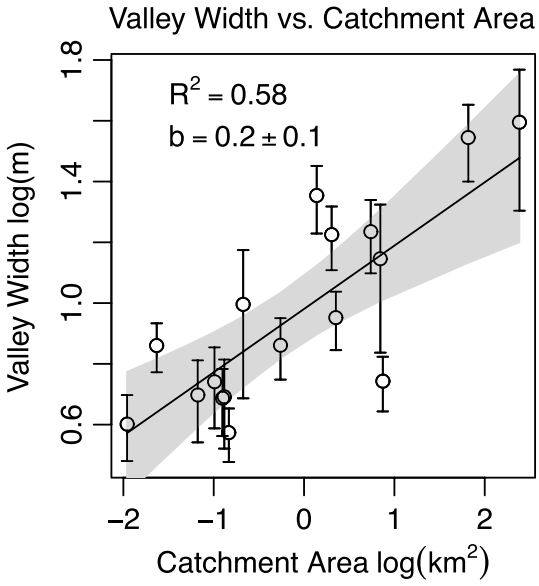

Figure 9. Plot of incised valley floor width versus catchment area. Error bars represent 1 standard deviation of width values derived from valley floor polygons digitized from SPOT5 imagery and analyzed according to the method of *Fisher et al.* [2013]. Valley width, W, increases with catchment size, A, as $W \propto A^b$, with exponent $b = 0.2 \pm 0.1$.

$$\omega = \rho_w g \frac{Q_w}{W} S_c. \tag{12}$$

ρ_w is the density of water in kg/m^3, and g is the gravitational acceleration in m/s^2. The dimensions for specific stream power are work per unit area per year, $Jm^{-2}yr^{-1}$. Following the approach of *Whipple and Tucker* [1999], we hypothesize that erosion rate follows a power law relationship similar to the approach for channel steepness (2),

$$E(Q_w, W, S_c) = k_e \omega^n. \tag{13}$$

This simple formulation for stream power erosion ignores the effects of variable flood size and frequency, as well as variable channel width, as discussed in *Lague* [2013]. Also, this approach is unlikely to be sufficient for channels eroded by debris flows [*Stock and Dietrich*, 2003]. These effects will be considered below in discussion of effective n values derived from our results.

Lacking data with which to constrain the characteristic discharge, we substitute a power function of upstream catchment area,

$$Q_w = k_q A^c, \tag{14}$$

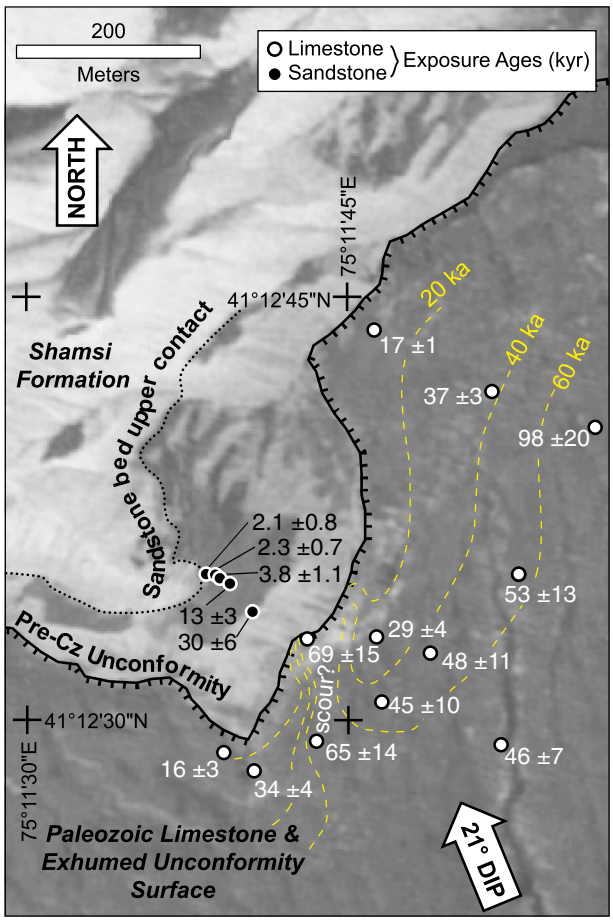

Figure 10. ^{36}Cl exposure ages from Baybeiche cuesta (see Figure 4 for location) show progressive stripping of Cenozoic cover strata, revealing resistant Paleozoic limestone beneath the unconformity. Ages shown here calculated assuming a surface-lowering rate of 7.5 mm/kyr. Background is orthorectified SPOT-5 panchromatic image. Yellow exposure age contours show interpreted positions through time of the unconformity between Cenozoic and Paleozoic rocks. Anomalously old age from Paleozoic limestone near contact with Cenozoic strata may be due to localized channel scour that prematurely exposed the limestone. Ages are also shown for exposure of a resistant sandstone bed within the lowermost Shamsi formation. These ages are consistent with the overall rate of exposure of the limestone, below, and together the suite of data support an overall steady state northward retreat of the cuesta.

where the area discharge exponent, c, is a value close to unity and k_q is a constant with units of m^3/km^{2c}. Combining (12), (13), and (14) and dividing through by V yields an expression of stream power in terms of dimensionless incision rate, similar in form to (10),

$$I = \frac{E}{V} = \frac{k_e}{V}\left(\rho_w g k_q \frac{A^c}{W} S_c\right)^n. \tag{15}$$

Taking the logarithm of each side and grouping terms,

$$\log(I) = \log\left(\frac{K}{V}\right) + n\log\left(\frac{A^c}{W} S_c\right), \tag{16}$$

where K in this instance is the product, $k_e(\rho_w g k_q)^n$.

Figure 12 shows the correlation of all of the channels for which valley width measurements were made from satellite imagery. It is assumed that $c = 1$. Once again there is a positive correlation with incision, and the fit to the data has slightly improved ($R^2 = 0.70$). The value of n determined from the slope of the relationship has dropped significantly, to 0.5 ± 0.2. This reflects the low scaling exponent for valley width that we determined from our satellite measurements (Figure 9). Substituting a power law relationship for valley width, $W = k_w Q_w^b$, consistent with the relationship shown in Figure 9 into (16) yields an expression,

$$\log(I) = \log\left(\frac{K}{V}\right) + n\log(A^{c(1-b)} S_c), \tag{17}$$

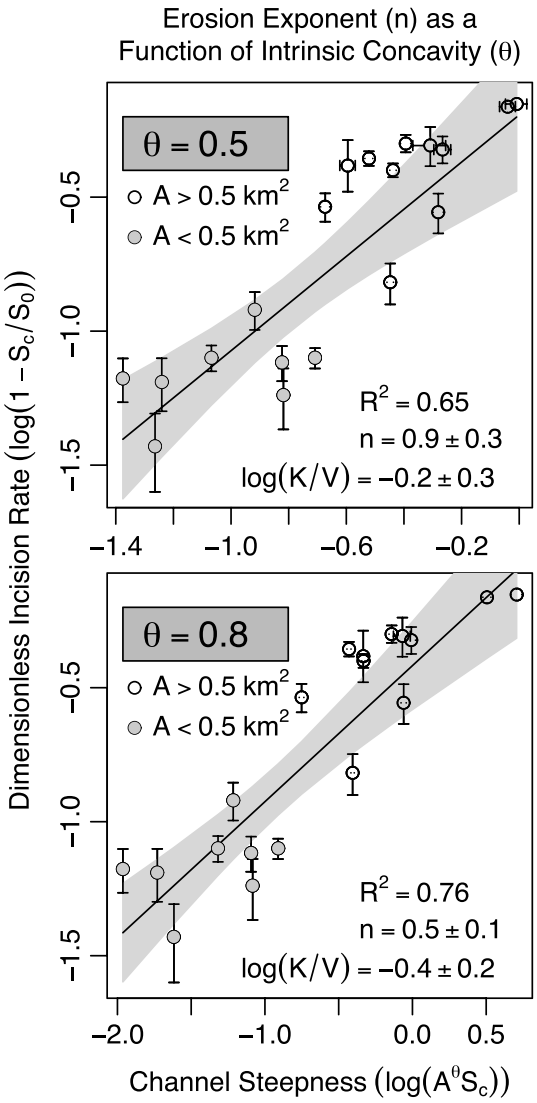

Figure 11. Plots of dimensionless erosion rate (I) versus channel steepness (k_s) for values of (top) $\theta = 0.5$ and (bottom) $\theta = 0.8$. Least-squares regression slopes indicate values of the exponent, n, for the relationship of erosion rate to channel steepness. Error bars and shaded areas show 95% confidence of values and regression lines, respectively.

that is the same as the empirical relationship for channel steepness (10) with $K = k_e(\rho_w g k_w^{-1} k_q^{(1-b)})^n$ and the intrinsic concavity $\theta = c(1 - b)$. As discussed in *Whipple* [2004], among others, this shows how exponent θ is largely controlled by the channel width scaling exponent, b. A globally typical value of $b \approx 0.5$ yields $\theta \approx 0.5$ [*Whipple*, 2004], whereas our finding of $b = 0.2 \pm 0.1$ for valley width in this particular field setting yields $\theta = 0.8 \pm 0.1$ (assuming $c = 1$). Figure 11 (bottom) shows the same incision rate versus channel steepness relationship as in Figure 11 (top), except that the intrinsic concavity has been raised from 0.5 to 0.8. As in Figure 12, the slope of the relationship indicating the value of n has declined, to 0.5 ± 0.1.

It has been suggested from observations [*Duvall et al.*, 2004; *Finnegan et al.*, 2005] and numerical modeling [*Wobus et al.*, 2006b] that channel width should narrow with channel slope (and thus with incision rate) in addition to increasing with catchment area and discharge. Unfortunately, our valley width data are insufficient to determine whether a negative correlation with channel slope exists in addition to the positive correlation with catchment area (Figure 9). If channel width narrowing does occur, then channels do not need to be as steep for the same incisional power. This increases the effective value of n.

5.2. Interpretation of Effective *n*

The collected slope and catchment area data from progressively exposed bedrock on the Baybeiche range provides a distribution of data sufficient to evaluate the relationship of incision rate to channel steepness and extract likely values for the unknown power law exponent, n (Figures 11 and 12). However, the value of θ used in our analysis should be treated as tentative, for two reasons. First, the area discharge exponent, c, is unconstrained, and second, it is uncertain whether our valley width data adequately capture the distribution of channel erosion across valley floors versus other competing processes of valley width adjustment such as collapse of valley walls or incision by debris flows. Nonetheless, a conservative interpretation of our results supports low n values between 0.5 and ~1.0. Values of n significantly greater than unity are not supported by our data set.

Further resolution of the values of n and the ratio of the rate constant K to the lowering rate of the cover strata, V, is limited by uncertainty of the channel and unconformity slope data. Only errors in slope measurements are considered here, because we assume no significant random error is associated with the digitization of catchment areas. The effects of the uncertainty in these slope calculations are shown as the error bars in Figures 11 and 12. Errors in the calculation of dimensionless incision, I, are greatest for small catchment areas, where channel slope is only slightly less than the slope of the unconformity. This amplified error occurs because the error in the ratio S_c/S_0 becomes increasingly important as $I \rightarrow 0$.

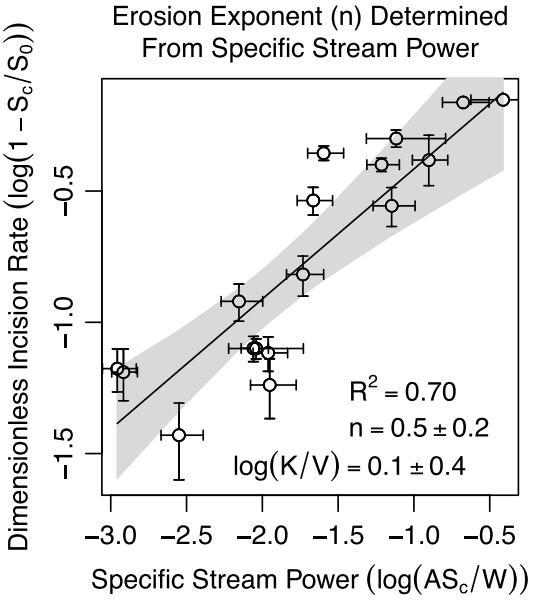

Figure 12. Plot of dimensionless erosion rate, *I*, versus specific stream power calculated for channels with valley width data. Least-squares regression slope indicates the exponent, $n = 0.5 \pm 0.2$, for the relationship of erosion rate to specific stream power. Error bars and shaded areas show 95% confidence of values and regression lines.

Conversely, errors in channel steepness are proportionally greater at larger catchment areas because channel steepness is more sensitive to slope than area, i.e., $\theta < 1$.

Despite the sometimes considerable errors, not all of the points overlap the best fit regression lines in Figures 11 and 12. The residual misfits suggest that controls from additional unconstrained factors, such as differences in runoff generation, rock strength, fracture spacing, or variability in the rate of stripping of the unconformity surface between sites. Errors in runoff generation, rock strength, or fracture spacing would have to have a significant effect (~50%) to provide the shift necessary to bring points into overlap with the regression lines. Error in digitization of the catchment area is likely to be small. The apparent under prediction or overprediction of dimensionless incision also does not correspond to geographic groupings of channels (Figure 4) and, therefore, argues against the role of rock strength, bedding orientation, or a variable rate of exposure of the unconformity, although the latter cannot be ruled out completely, as illustrated by the increase in spacing of age contours on the east side of the Baybeiche cuesta (Figure 10). Another possible and difficult-to-quantify source of error is the role of subsurface flow. Collapsed caverns and sapping features at the heads of valleys suggest that contributions from subsurface flow may significantly add to or intercept runoff in the studied catchments. Such features were avoided in surveys of smaller (<1 km^2) catchments but could have been overlooked in parts of the larger catchment areas.

The effective *n* values we find are low relative to results from other studies that focused on larger rivers [*Snyder et al.*, 2000, 2003; *DiBiase et al.*, 2010] that derived $n \geq 2$. We interpret our resulting low *n* values as an indication that discharge variability and the presence of an erosion threshold may be less important for small, steep streams than for larger rivers and drainage areas with less steep gradients and greater bed load transport. Even though the limestone bedrock is relatively resistant to erosion, the very steep channels incised into the Baybeiche range may regularly overcome thresholds for channel incision during moderate discharge events. Setting discharge variability effects aside and interpreting our results in terms of the physical processes of channel erosion, an erosion rate proportional to basal shear stress, with $n = 2/3$, falls well within the predictions of our data set. At the higher end, a value of $n = 1$, indicating channel incision rate proportional to total power expenditure per unit area of channel bed, is also supported from our data. However, any adjustment for variable runoff frequency or narrowing of channel width with increasing channel slope would make a value of $n = 1$ less likely. Regression of the steepness data using values of intrinsic concavity below 0.5 does yield *n* values greater than one, but with marked decrease of fit quality.

Because the channels measured from the Baybeiche range span a very wide range of catchment area, the processes that control incision of these channels are unlikely to be the same across all scales. This is evident from our field observations, which suggest that debris flows probably dominate erosion of the smallest catchments, whereas bed load cover increases considerably for the largest channels. We note that channels with very small catchment areas ($A < 0.25$ km^2) and very little incision ($I < 0.1$) define a trend that falls below the regression lines as channel steepness increases (Figure 11). Conversely, channels with larger catchment areas ($A > 0.5$ km^2) tend to have higher incision, even where their steepness or specific stream power is equivalent to that of smaller catchments with steeper channels. This contrast could indicate a transition from debris flow to more efficient fluvially dominated channel incision at catchment sizes greater than about 0.5 km^2. Alternatively, the smaller catchments may be tool starved compared to larger catchments.

Note that excluding channels with catchment areas below 0.5 km^2 from the regressions shown in Figure 11 would slightly decrease the effective *n* values.

5.3. Surface-Erosion Effects on ^{36}Cl Ages

Though the exhumed unconformity surface appears pristine (Figure 3), a slow rate of surface lowering by dissolution likely impacts its exposure history and resulting ^{36}Cl ages. Chemical erosion rates of carbonate rocks are strongly dependent on precipitation amount. Reported values based on outcrop or monument studies vary widely (especially since many modern observations are biased high by anthropogenic acidic rain), but typically vary between 5 mm/kyr under arid climate and 10–15 mm/kyr in temperate humid conditions, to as much as 150 mm/kyr under very wet tropical climate [*Guidobaldi and Mecchi*, 1993; *Meierding*, 1993; *Stone et al.*, 1994]. *Bluth and Kump* [1994] quantified the relation between annual runoff and bicarbonate flux for carbonate-dominated watersheds, using 20 watersheds. The correlation coefficient of 0.985 between runoff and flux indicates robust predictive ability. Precipitation in the Naryn River Valley is 300 mm/yr [*World Weather*, 2013]. Although runoff estimates are not spatially highly resolved, estimates in *Lvovitch* [1973] and *Sokolov* [1981] are in the range of 100 to 200 mm/yr. We have used 150 mm/yr as our best estimate, with a range of 100 to 200 mm/yr to explore the sensitivity of the exposure ages to plausible variation in erosion. Assuming that half of the calculated HCO_3 flux originates as gaseous CO_2, the formulation of *Bluth and Kump* [1994] produces a best estimate surface-denudation rate of 7.5 mm/kyr, with a range from 5 to 10 mm/kyr. Higher surface lowering rates require physical erosion, such as by frost cracking [*Tucker et al.*, 2011]. However, physical erosion would result in abundant angular clasts on the surface, whereas the unconformity outcrops are almost free of clasts and instead show small scale pitting and surface-rilling characteristic of chemical dissolution.

For samples with young exposure ages (<13 ka), variation of the surface lowering rate from 5 to 10 mm/kyr produced only very small changes in the ages (<7%). For older samples (with one exception), the maximum age variation was 15%, with most samples showing much less variation. This robust behavior of the calculated age in the face of substantial variation in erosion rate is because in these samples, the ^{36}Cl production is contributed approximately equally by spallation reactions and by low-energy neutron absorption by ^{35}Cl. Since the change in apparent age for these reactions is in opposite directions as erosion rate increases, the effects tend to cancel. The one exception to this pattern is sample KYR04-12, for which the age increase was 50%. This sample both had a long exposure and a low Cl concentration. Its sensitivity to erosion is more typical of a purely spallogenic nuclide such as ^{10}Be. When the assumed erosion rate is raised to 25 mm/kyr, similar to that found for limestone fault scarps in Italy [*Tucker et al.*, 2011], 8 of the 17 samples fail to yield an age because the measured ^{36}Cl concentrations exceed secular equilibrium values (i.e., infinite exposure time). These high ^{36}Cl concentrations strongly support the argument that very rapid, frost-shattering dominated erosion did not occur at this site at the elevations surveyed. For the sandstone samples, the same 7.5 mm/kyr rate of surface lowering as for the nearby limestone samples is assumed, although in detail this rate does not significantly affect these relatively young ages. In summary, within the bounds of reasonable and plausible surface erosion rate estimates, the calculated ^{36}Cl ages are not sensitive to erosion.

5.4. Calibration of the Erosion Rate Constant With ^{36}Cl

Altogether the distribution of surface exposure ages (Figures 4 and 10) supports the hypothesis of progressive stripping of the more erodible Cenozoic strata from the resistant Paleozoic limestone, resulting in the progressive exposure of the planar unconformity surface. To calibrate the rate of stripping for the Baybeiche cuesta site, exposure ages for both the limestone outcrops and the adjacent sandstone bed are plotted together in a graph of distance from the unconformity or upper contact, respectively, versus the sample age (Figure 13). Distances from each limestone outcrop to the unconformity are measured parallel to the dip direction of the unconformity surface. Distances for the sandstone samples measured along the sample transect are multiplied by 0.9, the cosine of the angle between this transect and the dip direction. Exposure ages from the sandstone samples together with nearby limestone samples are consistent with a stripping rate of ~2 m/kyr near the apex of the Baybeiche cuesta. Samples located along the east side of this cuesta indicate a higher rate stripping of ~4 to 6 m/kyr. Note this higher rate is also indicated by the wider spacing of age contours on Figure 10. This variability in stripping rate indicates nonuniform erosion at the local scale, possibly related to rearrangement of channel network geometry as bedrock is progressively exposed. For the Karatoo cuesta we find that the local rate of stripping, ~1 to 2 m/kyr, is slightly lower than that at the apex of the Baybeiche cuesta.

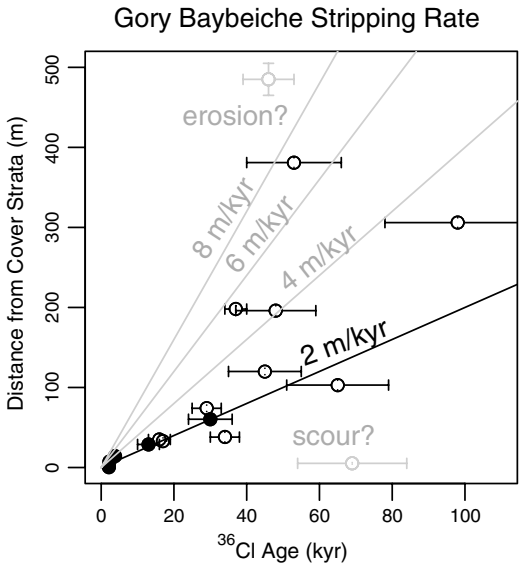

Figure 13. Interpretation of stripping rate of strata from the Baybeiche cuesta (see Figure 10 for sample map). Plot shows sample distance, measured horizontally, from the unconformity (white points, for exposure of limestone) or the inner edge of a resistant bed within the Shamsi formation (black points, for exposure of sandstone.). Light gray points are excluded samples that indicate either erosion of the limestone, producing anomalously young age, or possible early exposure due to channel scour through Cenozoic strata, producing anomalously old age. Overall, the ^{36}Cl exposure ages are consistent with a stripping rate of ~2 m/kyr near the apex of the cuesta since 60 ka, and somewhat higher rates of 4 to 6 m/kyr on its eastern side.

In the plots shown in Figures 11 and 12, the ratio of the limestone erosion-rate constant, K, to the erosion rate of the Cenozoic cover strata, V, has been determined from the predicted value of dimensionless incision, I, where the $\log(k_s) = 0$. By independently determining the rate of stripping of Cenozoic sedimentary rocks from the unconformity surface, as shown in Figure 10, one can further isolate values of K. Rates of stripping of 2 to 6 m/kyr, determined from exposure age dating (Figure 13), are transformed into a vertical rate of erosion by multiplying by the tangent of the dip of the unconformity surface. This manipulation yields a vertical rate of erosion of the cover strata, $V \approx 1$ m/kyr near the apex of the Gory Baybeiche cuesta, increasing to ≈2 m/kyr on its eastern side where the age contours are more widely spaced (Figure 10). The exposure age data for the Karatoo cuesta yield a lower erosion rate, 0.5 ± 0.2 m/kyr, averaged over a longer interval of time than at the Baybeiche cuesta (~200 kyr versus 60 kyr).

For a graded channel incising at a uniform steady rate (equation (3)), the ratio $(E/K)^{1/n}$ predicts the channel steepness [*Wobus et al.*, 2006a]. Here we use K values determined from the landscape of the Baybeiche Range to explore corresponding steepness values for such a graded channel. Both the value and units of K depend on the exponent, n. Rearranging either (10) or (15) and solving for the appropriate value of K/V yields

$$\frac{K}{V} = I \times k_s^{-n}. \tag{18}$$

Using $n = 1$ with intrinsic concavity, $\theta = 0.5$ yields values of $I \times k_s^{-n}$ ranging from 0.4 to 1.6 km^{-1} with mean of 0.9 ± 0.2 km^{-1} (2 standard error). Multiplying by the vertical rate of stripping for the cover strata, $V = 1$ m/kyr, and converting meter to kilometer yields a mean K value of $9 \pm 2 \times 10^{-4}$ kyr^{-1}. If instead erosion proportional to basal shear stress is employed ($n = 2/3$) with intrinsic concavity, $\theta = 0.75$ (chosen so that the units of K work out the same as for the specific stream power case), then values of $I \times k_s^{-n}$ range from 0.3 to 0.9 km^{-1} with one outlier of 1.2 km^{-1}. The mean, including this outlier, is 0.6 ± 0.1 km^{-1} (2 standard error), yielding a value for K of $6 \pm 1 \times 10^{-4}$ kyr^{-1} for V =1 m/kyr. For a graded channel eroding at a rate of 1 m/kyr, these values for K predict very high steepness values, with k_s, ranging from $1.1^{+0.3}_{-0.2} \times 10^3 m$ for the $n = 1$, $\theta = 0.5$ case, to $1.7 \pm 0.3 \times 10^3 m^{3/2}$ for the $n = 2/3$, $\theta = 0.75$ case. In such a hypothetical landscape, channel slopes exceeding 35° are predicted at catchment areas under 2.5 and 0.3 km^2, respectively.

Overall, the morphology of the Baybeiche Range and similar settings elsewhere in the Tian Shan [*Davis*, 1904] strongly reflects that channel incision becomes much less efficient for all but the largest streams once the limestone bedrock is exposed from beneath the cover strata. Relatively uniform and rapid lowering of the cover strata gives way to a spectrum of channel incision rates into bedrock that is correlated to catchment area. Only the largest two streams in the study area, D1 and D2, with the lowest gradients relative to the inclination of the unconformity surface (Figure 7), attain steepness values sufficient to erode the limestone close to 1 m/kyr. It is probable that the incision rate of these largest streams through the limestone bedrock sets the pace of overall lowering of the nearby Cenozoic strata. Tributary streams with lower catchment areas can keep pace while incising the cover strata, but cannot achieve a slope sufficient to incise limestone bedrock at the same rate.

6. Conclusion

Using channel incision into a previously tilted and progressively exposed unconformity between easily eroded versus erosionally resistant rocks, we calibrate the relationship of channel steepness to channel incision rate. Topographic measurements of channel slope and contact slope are presented from 19 channels incised into resistant limestone bedrock of the Baybeiche range in the western Tian Shan. By relating channel steepness to a dimensionless channel incision rate derived from the geometry of this progressively exposed boundary, we find low values, between 0.5 ± 1 and 0.9 ± 0.3, for the exponent, n, on the channel steepness erosion rate relationship. These effective n values are most consistent with incision proportional to basal shear stress ($n = 2/3$), although erosion proportional to specific stream power ($n = 1$) would also satisfy the data set. Our results show that a nonlinear relationship, with n significantly greater than one, is not acting on this landscape. This finding argues against significant impact from flood frequency or channel-narrowing effects, in this setting of low-order channels, that would tend to raise effective n values.

By measuring the rate of erosional stripping of the cover strata from the unconformity surface, we further isolate the erosion rate constant, K, for incision of the limestone bedrock below the unconformity surface. From cosmogenic ^{36}Cl exposure age dating, we determined rates of exposure between 2 and 6 m/kyr for the Baybeiche range, equivalent to a vertical rate of erosion of 0.5 to 2 m/kyr of the cover strata. Using a rate of 1 m/kyr, we find that the rate constant, K, ranges from 6×10^{-4} kyr^{-1} for the $n = 2/3, \theta = 0.75$ case to 9×10^{-4} kyr^{-1} for $n = 1, \theta = 0.5$ case. Altogether the analysis presented herein provides an observationally constrained confirmation of the power of channel steepness to predict erosion rate for landscape evolution where bedrock channels dominate.

Acknowledgments
We thank Kanat Abdrakhmatov and Cholponbek Ormukov of the Kyrgyz Institute of Seismology for their assistance with arranging for fieldwork in Kyrgyzstan. We also thank the Associate Editor D. Lague and reviewers A. Whittaker and G. Tucker. This research was supported by NASA (NAG5-13758, NNX08AG05G).

References

Abdrakhmatov, K. Y., et al. (1996), Relatively recent construction of the Tien Shan inferred from GPS measurements of present-day crustal deformation rates, *Nature*, *384*, 450–453.
Abdrakhmatov, K. Y., R. J. Weldon, S. C. Thompson, D. W. Burbank, C. M. Rubin, M. Miller, and P. Molnar (2001), Onset, style and current rate of shortening in the central Tien Shan (Kyrgyzstan), *Russ. Geol. Geophys.*, *42*(10), 1502–1526.
Beaumont, C., P. Fullsack, and J. Hamilton (1992), Erosional control of active compressional orogens, in *Thrust Tectonics*, edited by K. McClay, pp. 377–390, Chapman and Hall, London.
Bluth, G. J. S., and L. R. Kump (1994), Lithologic and climatologic controls of river chemistry, *Geochim. Cosmochim. Acta*, *58*, 2341–2359.
Bullen, M., D. Burbank, J. Garver, and K. Abdrakhmatov (2001), Late Cenozoic tectonic evolution of the northwestern Tien Shan: New age estimates for the initiation of mountain building, *Geol. Soc. Am. Bull.*, *113*, 1544–1559.
Burbank, D. W., J. K. McLean, M. Bullen, K. Y. Abdrakhmatov, and M. M. Miller (1999), Partitioning of intermontane basins by thrust-related folding, Tien Shan, Kyrgyzstan, *Basin Res.*, *11*, 75–92.
Chatanantavet, P., and G. Parker (2009), Physically based modeling of bedrock incision by abrasion, plucking, and macroabrasion, *J. Geophys. Res.*, *114*, F04018, doi:10.1029/2008JF001044.
Chediya, O. K. (1986), *Morphostructure and Neo-tectonics of the Tien Shan*, Frunze, Academia Nauk Kyrgyz CCP.
Cowie, P. A., A. C. Whittaker, M. Attal, G. P. Roberts, G. E. Tucker, and A. Ganas (2008), New constraints on sediment-flux-dependent river incision: Implications for extracting tectonic signals from river profiles, *Geology*, *36*, 535–538.
Crosby, B. T., K. X. Whipple, N. M. Gasparini, and C. W. Wobus (2007), Formation of fluvial hanging valleys: Theory and simulation, *J. Geophys. Res.*, *112*, F03S10, doi:10.1029/2006JF000566.
Davis, W. M. (1904), A flat-topped range in the Tian-Shan, *Appalachia*, *10*, 277–284.
Desilets, D., M. Zreda, P. Almasi, and D. Elmore (2006), Determination of cosmogenic Cl-36 in rocks by isotope dilution: Innovations, validation and error propagation, *Chem. Geol.*, *233*(3–4), 185–195.
DiBiase, R. A., and K. X. Whipple (2011), The influence of erosion thresholds and runoff variability on the relationships among topography, climate, and erosion rate, *J. Geophys. Res.*, *116*, F04036, doi:10.1029/2011JF002095.
DiBiase, R. A., K. X. Whipple, A. M. Heimsath, and W. B. Ouimet (2010), Landscape form and millennial erosion rates in the San Gabriel Mountains, California, *Earth Planet. Sci. Lett.*, *289*(1–2), 134–144.
Duvall, A., E. Kirby, and D. W. Burbank (2004), Tectonic and lithologic controls on bedrock channel profiles and processes in coastal California, *J. Geophys. Res.*, *109*, F03002, doi:10.1029/2003JF000086.
Farr, T. G., et al. (2007), The shuttle radar topography mission, *Rev. Geophys.*, *45*, RG2004, doi:10.1029/2005RG000183.
Finnegan, N. J., G. Roe, D. R. Montgomery, and B. Hallet (2005), Controls on the channel width of rivers: Implications for modeling fluvial incision of bedrock, *Geology*, *33*(3), 229–232.
Fisher, G. B., B. Bookhagen, and C. B. Amos (2013), Channel planform geometry and slopes from freely available high-spatial resolution imagery and DEM fusion: Implications for channel width scalings, erosion proxies, and fluvial signatures in tectonically active landscapes, *Geomorphology*, *194*, 46–56.
Flint, J. J. (1974), Stream gradient as a function of order, magnitude, and discharge, *Water Resour. Res.*, *10*(5), 969–973.
Goode, J. K. (2011), Interactions of tectonics and rivers with the surface, PhD thesis, University of California, Santa Barbara.
Goode, J. K., and D. W. Burbank (2011), Kinematic implications of consequent channels on growing folds, *J. Geophys. Res.*, *116*, B04407, doi:10.1029/2010JB007617.
Goode, J. K., D. W. Burbank, and B. Bookhagen (2011), Basin width control of faulting in the Naryn basin, South-central Kyrgyzstan, *Tectonics*, *30*, TC6009, doi:10.1029/2011TC002910.
Guidobaldi, F., and A. M. Mecchi (1993), Corrosion of ancient marble monuments by rain: Evaluation of pre-industrial recession rates by laboratory simulations, *Atmos. Environ. Part B*, *27*, 339–351.

Hancock, G. S., R. S. Anderson, and K. X. Whipple (1998), Beyond power: Bedrock river incision process and form, in *Rivers Over Rock: Fluvial Processes in Bedrock Channels*, edited by J. Tinkler and E. Wohl, pp. 35–60, AGU, Washington, D. C.
Haviv, I., Y. Enzel, K. X. Whipple, E. Zilberman, J. Stone, A. Matmon, and L. K. Fifield (2006), Amplified erosion above waterfalls and oversteepened bedrock reaches, *J. Geophys. Res.*, *111*, F04004, doi:10.1029/2006JF000461.
Howard, A. D. (1994), A detachment-limited model of drainage basin evolution, *Water Resour. Res.*, *30*(7), 2261–2285.
Kirby, E., and K. Whipple (2001), Quantifying differential rock-uplift rates via stream profile analysis, *Geology*, *29*, 415–418.
Kooi, H., and C. Beaumont (1996), Large-scale geomorphology: Classical concepts reconciled and integrated with contemporary ideas via a surface processes model, *J. Geophys. Res.*, *101*(B2), 3361–3386.
Lague, D. (2013), The stream power river incision model: Evidence, theory, and beyond, *Earth Surf. Processes Landforms*, *39*, 38–61, doi:10.1002/esp.3462.
Lague, D., and P. Davy (2003), Constraints on the long-term colluvial erosion law by analyzing slope-area relationships at various tectonic uplift rates in the Siwaliks Hills (Nepal), *J. Geophys. Res.*, *108*(B2), 2129, doi:10.1029/2002JB001893.
Lague, D., N. Hovius, and P. Davy (2005), Discharge, discharge variability, and the bedrock channel profile, *J. Geophys. Res.*, *110*, F04006, doi:10.1029/2004JF000259.
Lamb, M. P., W. E. Dietrich, and L. S. Sklar (2008), A model for fluvial bedrock incision by impacting suspended and bed load sediment, *J. Geophys. Res.*, *113*, F03025, doi:10.1029/2007JF000915.
Lifton, N., T. Sato, and T. Dunai (2013), Scaling in situ cosmogenic nuclide production rates using analytical approximations to atmospheric cosmic-ray fluxes, *Earth Planet. Sci. Lett.*, *386*, 149–160.
Lvovitch, M. I. (1973), The global water balance, *Eos Trans. AGU*, *54*(1), 28–42.
Marrero, S. S. (2012), Calibration of cosmogenic chlorine-36, PhD thesis, New Mexico Institute of Mining and Technology.
Meierding, T. C. (1993), Inscription legibility method for estimating rock weathering rates, *Geomorphology*, *6*, 273–286.
Oskin, M. E., and D. Burbank (2007), Transient landscape evolution of basement-cored uplifts: Example of the Kyrgyz Range, Tian Shan, *J. Geophys. Res.*, *112*, F03S03, doi:10.1029/2006JF000563.
Ouimet, W. B., K. X. Whipple, and D. E. Granger (2009), Beyond threshold hillslopes: Channel adjustment to base-level fall in tectonically active mountain ranges, *Geology*, *37*(7), 579–582.
Pritchard, D., G. G. Roberts, N. J. White, and C. N. Richardson (2009), Uplift histories from river profiles, *Geophys. Res. Lett.*, *36*, L24301, doi:10.1029/2009GL040928.
Seidl, M. A., and W. E. Dietrich (1992), The problem of channel erosion into bedrock, *Catena Supp.*, *23*, 101–124.
Sklar, L., and W. E. Dietrich (2004), A mechanistic model for river incision into bedrock by saltating bed load, *Water Resour. Res.*, *40*, W06301, doi:10.1029/2003WR002496.
Snyder, N. P., K. X. Whipple, G. E. Tucker, and D. J. Merritts (2000), Landscape response to tectonic forcing: Digital elevation model analysis of stream profiles in the Mendocino triple junction region, northern California, *Geol. Soc. Am. Bull.*, *112*(8), 1250–1263.
Snyder, N. P., K. X. Whipple, G. Tucker, and D. J. Merritts (2003), Importance of a stochastic distribution of floods and erosion thresholds in the bedrock river incision problem, *J. Geophys. Res.*, *108*, 2117, doi:10.1029/2001JB001655.
Sobel, E., M. Oskin, D. R. Burbank, and A. Mikolaichuk (2006), Exhumation of basement-cored uplifts: Example of the Kyrgyz Range quantified with apatite fission track thermochronology, *Tectonics*, *25*, TC2008, doi:10.1029/2005TC001809.
Sobel, E. R., and N. Arnaud (2000), Cretaceous-Paleogene basaltic rocks of the Tuyon basin, NW china and the Kyrgyz Tian shan: The trace of a small plume, *Lithos*, *50*, 191–215.
Sobel, E. R., and T. A. Dumitru (1997), Thrusting and exhumation around the margins of the western Tarim basin during the India-Asia collision, *J. Geophys. Res.*, *102*(B3), 5043–5063.
Sokolov, V. (1981), The biosphere reserve concept in the USSR, *Ambio*, *10*(2-3), 97–101.
Stock, J., and W. E. Dietrich (2003), Valley incision by debris flows: Evidence of a topographic signature, *Water Resour. Res.*, *39*(4), 1089, doi:10.1029/2001WR001057.
Stock, J. D., and D. R. Montgomery (1999), Geologic constraints on bedrock river incision using the stream power law, *J. Geophys. Res.*, *104*(B3), 4983–4993.
Stone, J. O. H., G. L. Allan, L. K. Fifield, J. M. Evans, and A. R. Chivas (1994), Limestone erosion measurements with cosmogenic chlorine-36 in calcite-preliminary results from Australia, *Nucl. Instrum. Methods Phys. Res., B92*, 311–316.
Tucker, G. E. (2004), Drainage basin sensitivity to tectonic and climatic forcing: Implications of a stochastic model for the role of entrainment and erosion thresholds, *Earth Surf. Processes Landforms*, *29*(2), 185–205.
Tucker, G. E., and K. X. Whipple (2002), Topographic outcomes predicted by stream erosion models: Sensitivity analysis and intermodel comparison, *J. Geophys. Res.*, *107*(B9), 2179, doi:10.1029/2001JB000162.
Tucker, G. E., S. W. McCoy, A. C. Whittaker, G. P. Roberts, S. T. Lancaster, and R. Phillips (2011), Geomorphic significance of postglacial bedrock scarps on normal-fault footwalls, *J. Geophys. Res.*, *116*, F01022, doi:10.1029/2010JF001861.
Whipple, K., and G. Tucker (1999), Dynamics of the stream-power river incision model: Implications for height limits of mountain ranges, landscape response timescales, and research needs, *J. Geophys. Res.*, *104*, 17,661–17,674.
Whipple, K. X. (2004), Bedrock rivers and the geomorphology of active orogens, *Annu. Rev. Earth Planet. Sci.*, *32*, 151–185.
Whipple, K. X., and G. E. Tucker (2002), Implications of sediment-flux-dependent river incision models for landscape evolution, *J. Geophys. Res.*, *107*(B2), 2039, doi:10.1029/2000JB000044.
Whittaker, A. C., P. A. Cowie, M. Attal, G. E. Tucker, and G. P. Roberts (2007), Bedrock channel adjustment to tectonic forcing: Implications for predicting river incision rates, *Geology*, *35*, 103–106.
Wobus, C., K. Whipple, E. Kirby, N. Snyder, J. Johnson, K. Spyropolou, B. Crosby, and D. Sheehan (2006a), Tectonics from topography: Procedures, promise, and pitfalls, in *Tectonics, Climate, and Landscape Evolution: Geological Society of America Special Paper 398: Penrose Conference Series*, edited by S. Willett et al., pp. 55–74, Geological Society of America, Boulder, CO.
Wobus, C. W., G. E. Tucker, and R. S. Anderson (2006b), Self-formed bedrock channels, *Geophys. Res. Lett.*, *33*, L18408, doi:10.1029/2006GL027182.
World Weather (2013). [Available at http://www.worldweatheronline.com/naryn-weather-averages/east-kazakhstan/kz.aspx.]
Yanites, B. J., and G. E. Tucker (2010), Controls and limits on bedrock channel geometry, *J. Geophys. Res.*, *115*, F04019, doi:10.1029/2009JF001601.